Polycystic disease caused by deficiency in xylosyltransferase 2, an initiating enzyme of glycosaminoglycan biosynthesis

Eduard Condac*, Robert Silasi-Mansat*, Stanley Kosanke†, Trenton Schoeb‡, Rheal Towner§, Florea Lupu*, Richard D. Cummings¶, and Myron E. Hinsdale*‖**

*Cardiovascular Biology Research Program, §Free Radical Biology and Aging Research Program, 825 Northeast 13th Street, Oklahoma Medical Research Foundation, Oklahoma City, OK 73104; †Department of Pathology, University of Oklahoma, 940 Stanton L. Young Boulevard, BMSB, Room 203, Health Sciences Center, Oklahoma City, OK 73104; ‡Department of Genetics, University of Alabama at Birmingham, Volker Hall, 402, 1670 University Boulevard, Birmingham, AL 35294-0019; ¶Department of Biochemistry, Emory University School of Medicine, 4001 Rollins Research Center, Atlanta, GA 30322; and ‖Department of Cell Biology, College of Medicine, University of Oklahoma Health Sciences Center, P.O. Box 26901, Oklahoma City, OK 73104

The basic biochemical mechanisms underlying many heritable human polycystic diseases are unknown despite evidence that most cases are caused by mutations in members of several protein families, the most prominent being the polycystin gene family, whose products are found on the primary cilia, or due to mutations in posttranslational processing and transport. Inherited polycystic kidney disease, the most prevalent polycystic disease, currently affects ≈500,000 people in the United States. Decreases in proteoglycans (PGs) have been found in tissues and cultured cells from patients who suffer from autosomal dominant polycystic kidney disease, and this PG decrease has been hypothesized to be responsible for cystogenesis. This is possible because alterations in PG concentrations would be predicted to disrupt many homeostatic mechanisms of growth, development, and metabolism. To test this hypothesis, we have generated mice lacking xylosyltransferase 2 (XylT2), an enzyme involved in PG biosynthesis. Here we show that inactivation of XylT2 results in a substantial reduction in PGs and a phenotype characteristic of many aspects of polycystic liver and kidney disease, including biliary epithelial cysts, renal tubule dilation, organ fibrosis, and basement membrane abnormalities. Our findings demonstrate that alterations in PG concentrations can occur due to loss of XylT2, and that reduced PGs can induce cyst development.

animal model | extracellular matrix | genetics | proteoglycans | cyst

D evelopment of cysts, most frequently in the kidneys and/or liver, is a hallmark of hereditary polycystic disease. Patients experience high morbidity from cyst rupture, infection, and/or destruction of normal tissue. The most common polycystic disease (at 1 in 500 births) and the most studied is autosomal dominant polycystic kidney disease (ADPKD), caused by mutations in either *PKD1* or *PKD2* (1–8). ADPKD patients develop decreased renal function, renal tubule dilation, and cysts, and 70% develop liver biliary cysts. Alterations in epithelial cell growth and development, fluid secretion, polarization, and/or apoptosis (7–11) have all been linked to cyst development and growth and are thought to arise from abnormalities in the extracellular matrix (ECM), basement membrane (BM), and cellular mechanosensing and signaling by the primary cilium (7–10, 12–20).

Proteoglycans (PGs) are located on the cell surface and in the ECM and consist of a core protein with heparan sulfate (HS), chondroitin sulfate (CS), and dermatan sulfate glycosaminoglycan (GAG) side chains assembled on select serines. They influence many fundamental biological processes, including cytokine and growth factor function, morphogen gradient formation, and BM homeostasis (21–24). Therefore, the reduction in PGs observed in tissues and cultured cells from ADPKD

patients and polycystic kidney disease (PKD) animal models (9, 10, 16, 18) correlates well with the cyst-associated epithelial abnormalities of dedifferentiation, proliferation, and increased cell turnover. Despite this strong link to ADPKD, the role of PGs in ADPKD and other polycystic diseases has not been systematically studied. We have investigated the role that PGs play in the development of human polycystic disease by inactivating xylosyltransferase 2 [(XylT2) Enzyme Commission no. 2.4.2.26], an enzyme shown to be involved in HS and CS biosynthesis (25–27). We have shown in an experimental model system that reduced PGs are cystogenic.

Results

Mice Lacking XylT2 Have Significantly Reduced Liver PGs. The XylT family consists of *XYLT1* and *XYLT2*. In mice, *Xylt2* mRNA is detected as a single transcript in a wide range of tissues, including the kidney, and it is the only XylT detected in the liver (Fig. 1*a*). This tissue distribution is similar to that in humans (28) and is consistent with XylT2 having an important function in liver and kidney homeostasis. Using gene targeting in embryonic stem cells, we deleted 94% of the coding sequence of the *Xylt2* locus [supporting information (SI) Fig. 6]. Heterozygous ($Xylt2^{-/+}$) matings yielded the expected Mendelian ratios of mice (data not shown). Livers from $Xylt2^{-/-}$ mice did not express either *Xylt2* mRNA (SI Fig. 7*a*) or *Xylt1* mRNA (data not shown) as measured by real-time RT-PCR analyses with total RNA. Therefore, based on the lack of *Xylt* mRNA and the loss of coding sequence, the $Xylt2^{-/-}$ livers were considered devoid of known XylTs. As expected, the kidneys expressed no detectable *Xylt2* mRNA (SI Fig. 7*b*). Unexpectedly, a slight decrease in *Xylt1* mRNA levels relative to controls was found (SI Fig. 7*c*), but was not significant. Mutant liver PG levels were substantially decreased, with HS levels 87% reduced compared with controls (Fig. 1*b* and SI Fig. 7*d*). In the mutant livers, we found that HS was absent in the sinusoids, whereas residual HS, most likely

Fig. 1. XylT2 deficiency causes loss of the majority of PGs in the liver. (a) Multitissue Northern blot analysis of the expression of *Xylt2* and *Xylt1*, which are 4.0 and 9.5 kb, respectively. (b) Liver HS disaccharide analysis in $Xylt2^{+/+}$ (n = 5) and $Xylt2^{-/-}$ (n = 4) mice. (c) HS immunohistochemistry in the livers of 4-month-old $Xylt2^{+/+}$ and $Xylt2^{-/-}$ mice. (Scale bars: 50 μm.) Asterisk indicates the lumen of the portal venules, and the arrowheads indicate staining near BECs. Arrow in $Xylt2^{+/+}$ indicates sinusoidal staining and in $Xylt2^{-/-}$ indicates absence of sinusoidal staining. +Hep, heparitinase I-treated; −Hep, heparitinase I-untreated. (d) Western blot analysis of extracted liver protein for decorin in $Xylt2^{+/+}$ and $Xylt2^{-/-}$ mice. + above the lanes indicates sample treatment with chondroitinase ABC. Dec+ and Dec− are the decorin with and without attached GAG side chains, respectively. Numbers to the right are molecular weight standards in kDa. GAPDH is loading control.

from *Xylt1* expression, was present in the liver vasculature and in the portal triad regions (Fig. 1c). Significantly, although Northern blot analysis and real-time RT-PCR of total RNA showed the liver to have absent *Xylt1*, residual *Xylt1* mRNA was demonstrated with real-time RT-PCR by using poly(A) RNA as a template (SI Fig. 8). Predictably, the core proteins in the sinusoids should lack GAG side chains, and indeed Western blots on extracted proteins using an antibody against decorin showed that the mutants expressed decorin at levels similar to controls, but mostly lacked GAG side chains (Fig. 1d). Therefore, the $Xylt2^{-/-}$ mice have a deficit of PGs in the liver due to a loss of GAG side chains.

$Xylt2^{-/-}$ Mice Develop Liver Cysts. Despite relatively normal hepatic development, numerous cysts were found beginning at 4 to 5 months of age in 50% of the $Xylt2^{-/-}$ livers in males and females. No cysts were found in sibling controls (Fig. 2 a and b). Most cysts by gross examination appeared to emerge from within the liver and not the extrahepatic biliary tract. The portal triad areas in noncystic portions of mutant liver contained increased cell numbers relative to controls arising from biliary epithelial cell (BEC) hyperplasia and small basophilic mononuclear cells speculated to be inflammatory or oval cells (Fig. 2 a and b). Oval cell proliferation often accompanies BEC hyperplasia after liver injury (29). However, these cells were found to be CD45-positive inflammatory cells (Fig. 2 c and d). Furthermore, the liver portal triad areas showed increased fibrosis that diminished in the sinusoidal areas surrounding the portal triad (Fig. 2e). Mutant liver weights were significantly greater than controls even when the livers were cyst-free at 3 to 5 months of age and in 10-month-old animals with no liver cysts or in livers drained of cystic fluid (Fig. 2g). The liver cysts were susceptible to rupture,
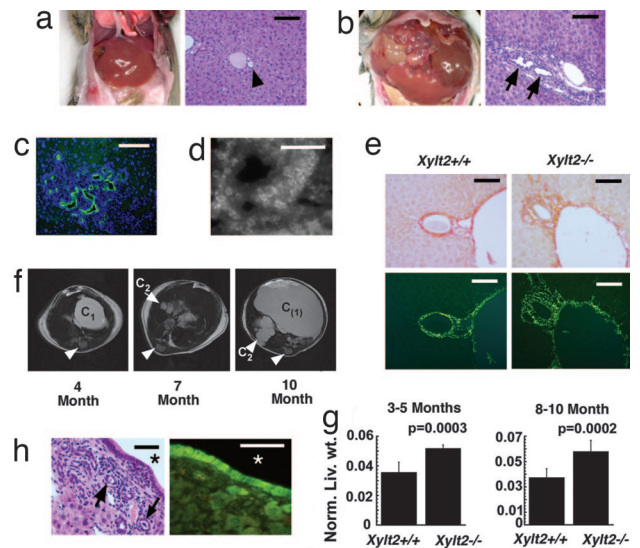

Fig. 2. XylT2 deficiency causes biliary tract hyperplasia and cysts. (a) $Xylt2^{+/+}$ liver. Gross liver (*Left*) and H&E staining (*Right*) of a portal triad. Arrowhead indicates biliary tract. (Scale bar: 100 μm.) (b) $Xylt2^{-/-}$ liver. Gross liver with cysts (*Left*) and H&E staining (*Right*) of portal triad area. Arrows show hyperplastic biliary tract. (Scale bar: 100 μm.) (c) Immunohistochemistry with oval cell/BEC marker antibody A6 of $Xylt2^{-/-}$ hyperplastic biliary epithelium. (Scale bar: 100 μm.) (d) CD45 marker immunohistochemistry of cells surrounding the hyperplastic biliary epithelium. (Scale bar: 50 μm.) (e) Sirius red staining for collagen. (*Upper*) Bright field and epipolarized light microscopy. (*Lower*) Same section examined with epipolarized light only. $Xylt2^{-/-}$ mouse portal triad shows increased periportal fibrous connective tissue as red-amber structures (*Upper*) and green shimmering structures (*Lower*). (Scale bars: 100 μm.) (f) MRI analyses of liver cysts in the same mutant female animal at different ages. Arrowheads indicate the spinal cord. C_1 indicates a liver cyst that was present at 4 months of age and virtually absent at 7 months of age. C_2 indicates a new cluster of cysts at 7 months of age that is still present and enlarged at 10 months of age. $C_{(1)}$ indicates either the healing and refilling of C_1 or a new cyst in the 10-month-old mutant liver. (g) Liver weight normalized to body weight at 3–5 ($Xylt2^{+/+}$, n = 8; $Xylt2^{-/-}$, n = 5) and 8–10 ($Xylt2^{+/+}$, n = 8; $Xylt2^{-/-}$, n = 6) months of age. (h) (*Left*) H&E staining of mutant liver cyst wall. Asterisk is lumen of cyst, and arrows show hyperplastic biliary epithelium and tracts in the wall of the cyst. (*Right*) Cytokeratin-19-positive BEC in a liver cyst. Asterisk indicates cyst lumen. (Scale bars: 50 μm.)

as shown by sequential MRI scans (Fig. 2f). The cystic fluid was generally clear and acellular, but was occasionally brown and rarely green tinged, suggesting the presence of blood or bile, respectively. The walls of the cysts were lined with cuboidal-columnar cytokeratin-19-positive BECs (Fig. 2h). Below the BECs was a layer of fibrous connective tissue containing collagen (Fig. 2h and SI Fig. 9) and hyperplastic biliary tracts containing and surrounded by small basophilic mononuclear cells, similar to those in the triad areas. Despite these abnormalities, liver enzymes were normal (see *Materials and Methods*, data not shown). Therefore, XylT2 deficiency results in significant liver abnormalities, including biliary tract hyperplasia, liver fibrosis, and biliary cysts that initiate and progress with age. However, despite these abnormalities, liver development and function are normal. These features closely resemble many of those observed in livers of ADPKD patients (9, 30, 31).

$Xylt2^{-/-}$ Mice Develop Renal Defects. The hallmark renal lesion in human ADPKD is dilation of renal tubules progressing to cyst development (8). The 9- to 10-month-old male $Xylt2^{-/-}$ mice had varying numbers of dilated tubules localizing primarily to the kidney cortex (0/8 $Xylt2^{+/+}$, 4/7 $Xylt2^{-/-}$; P = 0.03). Some had extensive tubular involvement, but the majority had at most one to two dilated tubules lined with cuboidal epithelium, suggesting

MEDICAL SCIENCES

www.manaraa.com
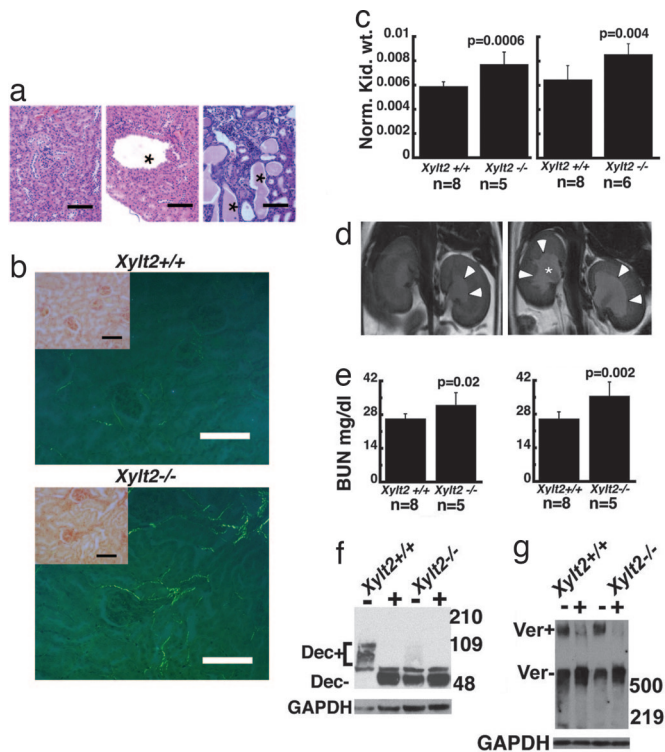
Fig. 3. XylT2 deficiency results in abnormal kidney function and structure. (*a*) (*Left*) Normal renal tubules in $Xylt2^{+/+}$ mice. (*Center*) Dilated $Xylt2^{-/-}$ tubule. Asterisk indicates the tubule lumen. (*Right*) $Xylt2^{-/-}$ tubule dilation and atrophy. Asterisk indicates the tubule lumens. (Scale bars: 100 μm.) (*b*) Sirius red staining as in Fig. 2*e* of renal cortex. (*Inset*) Bright field and epipolarized analyses. $Xylt2^{-/-}$ kidneys have increased fibrosis. (Scale bars: 100 μm.) (*c*) Kidney weights normalized to body weight in 3- to 5-month-old mice (*Left*) and 8- to 10-month-old animals (*Right*). (*d*) MRI kidney images from $Xylt2^{+/+}$ (*Left*) and $Xylt2^{-/-}$ (*Right*) mice. Arrowheads illustrate the renal pelvis, and asterisk indicates the renal papilla. (*e*) BUN in 3- to 5-month-old (*Left*) and 10-month-old (*Right*) mice. (*f*) Western blot analysis using a decorin-specific antibody on extracted kidney proteins digested with (+) or without (−) chondroitinase ABC. Dec+ and Dec− are decorin with and without GAGs, respectively. Numbers to the right are molecular weight standards in kDa. GAPDH is loading control. (*g*) Versican Western blot of extracted kidney proteins incubated with and without chondroitinase ABC as indicated by plus and minus signs, respectively. Ver+ and Ver− are versican with and without GAGs, respectively. Numbers to the right are molecular weight standards in kDa. GAPDH is loading control.

Fig. 4. XylT2 deficiency induces PKD-like changes in BMs as seen by transmission EM. Asterisks indicate the lumen of the biliary canal or, in the case of the $Xylt2^{-/-}$ mice (*d–f*), the cystic lumen. (*a*) $Xylt2^{+/+}$ BECs lining a biliary tract. Microvilli can be seen in the lumen at the epithelial cell apical membranes. (Scale bar: 2 μm.) (*b*) $Xylt2^{+/+}$ BEC apical and basolateral surfaces. Basolateral junction of plasma membrane is slightly undulated, and the BM is clearly defined and uniform in thickness (arrows). (Scale bar: 500 nm.) (*c*) $Xylt2^{+/+}$ BEC apical and lateral junction of two BECs showing apical microvilli, tight junctions (arrowheads), and normal membranous junction between cells. (Scale bar: 500 nm.) (*d*) Cyst-associated BECs showing apical microvilli and secretory vesicles/granules (Sg). (Scale bar: 2 μm.) (*e*) Basolateral portion of BEC showing the lateral plasma membrane projections (Lp) and discontinuous, indistinct, and thickened BM (arrows). Collagen (col) deposition is also observed. (Scale bar: 500 nm.) (*f*) $Xylt2^{-/-}$ apical portion of cyst-associated BECs showing normal-appearing tight junctions (arrowheads) and microvilli, but, in contrast to controls, the presence of secretory granules (Sg). (Scale bar: 500 nm.)

that dilation was not due to increased pressure (Fig. 3*a*). Because there was no evidence that the dilated segments had separated from the nephron, these structures were not considered cysts. Interstitial fibrosis was observed throughout the mutant kidneys (Fig. 3*b*). These findings are similar to the range of incidence and severity of renal abnormalities in $Pkd1^{-/+}$ and $Pkd2^{-/+}$ knockout mice (32). Furthermore, at 3 and 10 months of age, kidneys of the $Xylt2^{-/-}$ mice weighed significantly more than those of controls (Fig. 3*c*). We observed a significant increase in hydronephrosis grossly (SI Fig. 10) and histologically in 6- to 7-month-old mutants (six of eight animals; $P = 0.007$) and in 9- to 10-month-old mutants (five of seven animals; $P = 0.04$) compared with zero affected age-matched controls. MRI analysis showed a similar increase in hydronephrosis at 11 to 12 months of age (0/7 $Xylt2^{+/+}$, 7/8 $Xylt2^{-/-}$; $P = 0.001$) (Fig. 3*d*). No other urinary tract abnormalities were observed, suggesting that the hydronephrosis was not due to physical urinary outflow obstruction. We hypothesize that the hydronephrosis may develop because the structural integrity of the renal pelvis might be affected by global XylT2 deficiency. The $Xylt2^{-/-}$ mice exhibited

reduced renal function shown as a significant increase in blood urea nitrogen (BUN) in younger (21% increase) and older (36% increase) animals (Fig. 3*e*). Because this increase in BUN levels is seen in the younger animals in the absence of hydronephrosis, a primary kidney defect unrelated to the hydronephrosis is likely. Similar to the liver, the mutant kidneys contained substantial GAG-free core protein (Fig. 3*f*), in contrast to normal total GAG levels as measured by alcian blue precipitation (SI Fig. 11). This finding suggests that renal decorin is more dependent on XylT2 activity than other core proteins. Normal renal versican modification levels (Fig. 3*g*) and similar levels of renal CS and HS in mutants and controls support this conclusion (SI Figs. 12 and 13). We speculate that the lack of overt tubule cysts suggests compensatory XylT1 activity in the kidney.

$Xylt2^{-/-}$ Mice Cystic BMs Resemble Those in PKD. In ADPKD patients, renal epithelial tubule BM thickening and lamination with loss of protein homogeneity are postulated to cause cyst development and progression (9, 12, 14, 17, 33). In the cystic BM of the $Xylt2^{-/-}$ mice, we observed several consistent ultrastructural abnormalities (Fig. 4). The basolateral junctions of mutant BECs have membranous lateral projections that interdigitate with those of adjacent cells (Fig. 4 *b* and *e*). These lateral projections appear similar to those described in early characterizations of the PKD mouse model *Cys-1^{cpk}* (34). The mutant BEC BM, in contrast to the uniform and easily visible control BM, has sections that are diffuse, indistinct, and thickened (Fig. 4 *b* and *c*). The apical portions of the mutant BECs contain tight
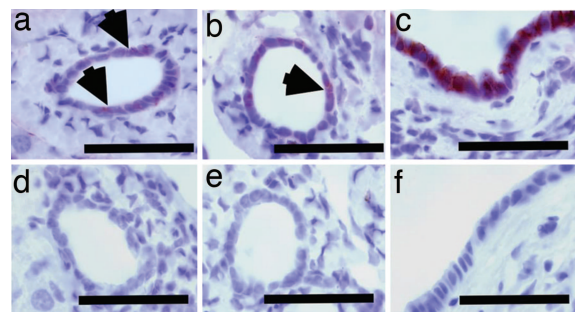
Fig. 5. Cystic biliary epithelium in *Xylt2*$^{-/-}$ mice has increased β-catenin. (*Upper*) Sections incubated with primary antibody. (*Lower*) Sections incubated without primary antibody. (*a* and *d*) Periodic light staining of BECs in *Xylt2*$^{+/+}$ biliary tract (arrowheads). (*b* and *e*) Some biliary tracts in *Xylt2*$^{-/-}$ mice are similar to controls in size and for β-catenin reactivity (arrowhead). (*c* and *f*) *Xylt2*$^{-/-}$ cystic wall BECs showing intense β-catenin staining. (Scale bars: 50 μm.)

junctions similar to the controls, but some of the cells have secretory-appearing vesicles not seen in control BECs (Fig. 4 *c*, *d*, and *f*). Because epithelial secretion is an important component of cyst development and progression (9), this finding is significant. We conclude that XylT2 deficiency causes ultrastructural changes in the cyst-associated BECs and their BM similar to those seen in PKD animal models and ADPKD.

Cystic Epithelium in *Xylt2*$^{-/-}$ Mice Has Increased β-Catenin. Transgenic mice overexpressing β-catenin develop cysts (35), and abnormalities in cellular signaling involving β-catenin are likely mechanistically involved in cyst development (7). Similarly, we observed increased β-catenin in the cystic epithelial cells in the mutant (Fig. 5). Therefore, cystic BECs' β-catenin expression in *Xylt2*$^{-/-}$ mice is likely important mechanistically in cyst development.

Discussion

In this paper, we find that *Xylt2* inactivation causes severe reduction in liver PG content. Despite this reduction, the *Xylt2*$^{-/-}$ mice develop normally. However, the mice develop liver biliary epithelial cysts, renal tubule dilation/cysts, and decreased renal function. These changes are very similar to those of PKD patients. We have shown previously that XylT2, the product of the *Xylt2* locus, is important in PG biosynthesis in many cell types (25), and in this paper we show that *Xylt2* mRNA is widely expressed as a single transcript. In addition to BEC hyperplasia and cyst development, *Xylt2* deficiency results in ultrastructural changes in the BEC BM and basolateral and apical portions of the cell, all of which are supportive of a role of XylT2-dependent PGs in the development of cysts.

The mechanism of the decreased PG in PKD is unknown. It could be rooted in increased degradation and/or reduced biosynthesis. Recent renal expression profiling from human ADPKD kidneys shows that matrix metalloprotease 1 expression increases and the PG biosynthetic enzyme β1,3-glucuronyltransferase 3 decreases in ADPKD (36). In addition, increased metalloprotease activity has been measured in PKD patient and animal model tissues (8, 18, 37). Because XylT2 and XylT1 catalyze the initial and proposed rate-limiting step of PG biosynthesis, a role of XylT activity in the pathogenesis of PKD is plausible. Could there be a subpopulation of PKD patients that may have a mutant *XYLT* responsible for cyst development? It is unlikely because most cases of PKD are a result of a *PKD1*, *PKD2*, or *PKHD1* mutation. Nonetheless, linkage analysis of *XYLT* polymorphisms with PKD patients has not been reported. More likely there is a larger PKD patient subgroup with known

PKD1, PKD2, or *PKHD1* mutations with linked *XYLT* polymorphisms associated with decreased enzyme activity resulting in a particular clinical picture (e.g., liver cysts in addition to renal cysts). In these cases, the mutated *XYLT* allele and product would be a genetic modifier of the PKD phenotype. Alternatively, alterations in the activity of other downstream enzymes of PG biosynthesis (e.g., β1,3-glucuronyltransferase 3) by defective polycystin-1 signaling could reduce PG biosynthesis, leading to cyst development.

Many PKD animal models have expedited the search for pathologic mechanisms of cyst development as well as for treatments (7, 38). The *Xylt2*$^{-/-}$ mice are a unique PKD animal model. PKD animal models have been indispensable in correlating dysfunctional primary cilia proteins with PKD (7, 20, 38). Other models show that proteins involved in biological processes ranging from cell cycle to gene transcription can be cystogenic (7, 38). Hypomorphic mutated laminin α-5 is the only ECM-associated protein mutation known to cause PKD (19). The *Xylt2*$^{-/-}$ mice show that decreased PGs can cause cyst development.

As with other PKD models, the *Xylt2*$^{-/-}$ mice reveal important aspects of basic biology. Several intriguing biological facts about the role of PGs in organ development and homeostasis are observed. First, the fact that liver development occurs in these mice is significant because liver PGs are influential in hepatocellular differentiation (39–41). XylT2 deficiency drastically reduces hepatocyte PG biosynthesis and has less effect on the vasculature and portal triad PG levels. Our results suggest that these residual PGs are sufficient for hepatocellular differentiation or that hepatocytes *in vivo* need minimal levels of PGs for development and maturation. Furthermore, given the widespread mRNA expression of *Xylt2*, that organogenesis and subsequent embryonic development can occur in the absence of XylT2 function is interesting. Second, despite such a reduction in PGs in the livers of the *Xylt2*$^{-/-}$ mice, the liver functions relatively normally. Third, although the kidney has expression of both *Xylt2* and *Xylt1*, it has functional as well as structural changes presumably due to the lack of XylT1 to compensate partially or fully for the absence of XylT2 function. This lack of compensation could be due to differences in substrate kinetics as well as cell type-specific expression of *Xylt1*. We do know that many cell types express both enzymes (25) and can plausibly up-regulate XylT1 activity to compensate for the loss of XylT2 function if the enzymes can share substrates. The preferential lack of modification of decorin illustrates that some core proteins may be more severely affected than others. These core proteins are potential mechanistic candidates linking reduced PG to cyst develop.

Whether PG homeostasis can be causally linked to ADPKD cyst development has been the subject of debate (16). Our findings indicate that decreased PG concentrations are cystogenic. Our data suggest that β-catenin is involved, and we hypothesize that lack of ECM-sequestered growth factors may induce β-catenin activity and proliferation of BECs. With regard to polycystin dysfunction, we speculate that lack of downstream cilia-signaling events may influence ECM composition by decreasing PG biosynthesis and/or increasing degradation, leading to cystogenic changes in epithelial cells. Alternatively, polycystin-1 (PC-1) may require cilia-associated or ECM PGs for optimal function because PC-1 has multiple extracellular domains suspected to interact with the ECM and other cell surface-associated proteins (8). In support of this hypothesis is the fact that GAG side chains are important in many protein–protein interactions (22, 42). These possibilities will be addressed in future studies.

Materials and Methods

Generation of *Xylt2*$^{-/-}$ Mice. A bacterial artificial chromosome fragment encompassing most of the *Xylt2* locus (Research Genetics, Huntsville, AL) was used to make the targeting

MEDICAL SCIENCES

www.manaraa.com

construct. The targeting scheme removed ≈9.5 kb from the locus and ≈94% of the coding sequence. See *SI Materials and Methods* for experimental details. The Institutional Care and Use Committee of the Oklahoma Medical Research Foundation approved all experiments and procedures with the mice.

Northern Blot, RT-PCR. Multitissue expression measurements by Northern blot analyses were performed by using a multitissue poly(A) Northern blot (MessageMap blot; Stratagene, La Jolla, CA). cDNA probe templates were 1.5 kb for *Xylt2* and 0.5 kb for *Xylt1*, both encoding the final coding sequence of the cDNA sequence, including the stop codon at the 3′ end. First-strand biosynthesis with RT was performed by using 2.5 μg of total or 0.5 μg of poly(A) RNA using oligo(dT) primer (Invitrogen, Carlsbad, CA). Real-time PCR was performed with standard techniques (SYBR Green PCR; Applied Biosystems, Foster City, CA) by using an ABI Prism 7000 Sequence Detection System PCR machine. See *SI Materials and Methods*.

Slide Preparation, Staining, Immunohistochemistry, and EM. For EM, fresh tissue was taken from animals, cut into 1-mm^3 tissue pieces fixed in 2% glutaraldehyde, and postfixed in 1% osmium tetroxide in 0.1 M caccodilate buffer. All tissues were treated with tannic acid in 0.1 M caccodilate buffer, followed by dehydration and flat embedding in Epon (EMBed-812; Electron Microscopy Sciences, Hatfield, PA). Areas of interest were identified by light microscopy analyses of semithin sections. Ultrathin sections were collected on copper-palladium grids and double stained with uranyl acetate and lead citrate, followed by EM analysis. For liver immunohistochemistry with F69–3G10 anti-HS antibody (Seikagaku America, Rockville, MD) for heparitinase-digested HS, the paraformaldehyde-fixed tissues were embedded in OCT compound (Raymond Lamb, Durham, NC) and sectioned. Sections were digested with heparitinase I (Seikagaku America) or incubated in buffer alone for 3 h at 37°C, followed by incubation with primary antibody (1:50) and reacted by using the M.O.M. peroxidase kit (PK-2200) and NovaRED (Vector Laboratories, Burlingame, CA) according to the manufacturer's instructions. Sections were counterstained with hematoxylin QS (Vector Laboratories). Oval cell immunohistochemistry was done by using the A6 antibody (43) generously provided by Valentina Factor (National Cancer Institute/National Institutes of Health, Bethesda, MD). This antibody recognizes both BEC and oval cells. It was used at a 1:10 dilution, followed by a secondary donkey anti-rat IgG Cy3 antibody (Jackson ImmunoResearch Laboratories, West Grove, PA) on frozen sections. CD45 antibody (BD Biosciences PharMingen, San Diego, CA), CK19 antibody (ab15463; Abcam, Cambridge, MA), sirius red stain, β-catenin antibody (BD Biosciences Transduction Laboratories, Lexington, KY), anti-HS F58–10E4 antibody, and anti-CS 2B6 antibody analyses were performed on paraffin-embedded sections, followed by counterstaining with hematoxylin QS (Vector Laboratories). See *SI Materials and Methods*.

PG Extraction and Western Blot Analyses. PGs were isolated from tissues by extraction with 7M Urea, 0.1 M NaCl, 50 mM Tris·HCl (pH 7.5), protease inhibitors (cat: 11–836-153–001; Roche Diagnostics, Indianapolis, IN), and 0.5% Triton X-100. Sample protein concentration was determined by using the Bradford assay (Pierce Chemical, Rockford, IL). General sample processing included dilution of 1:10, followed by digestion overnight with 0.29 units per ml of chondroitinase ABC (Seikagaku America) in Hepes 50 mM (pH 7.0), 0.1 M NaCl, 1 mM CaCl$_2$, and 15 mM benzamidine at 37°C. Fifteen to forty micrograms of protein was denatured, reduced, and separated by polyacryl-amide gel electrophoresis, followed by transfer to PVDF membrane (Westran 0.45 μm; Schleicher & Schuell, Keene, NH). Immunodetection was achieved with anti-decorin LF-113 (44) (a kind gift from Larry Fisher, National Institutes of Health, Bethesda, MD), anti-versican (GAG β-domain; Chemicon International, Temecula, CA), or anti-versican V0/V1 antibodies (a kind gift from Maria T. Dours-Zimmermann, University of Zurich, Zurich, Switzerland) (45). For a loading control, glyceraldehyde-3-phosphate dehydrogenase antibody (ab9485; Abcam) was used and detected with chemiluminescence (Millipore Corporation, Billerica, MA). See *SI Materials and Methods*.

Glycosaminoglycan Isolation, Measurements, and Polysaccharide Analyses. To estimate total GAGs, PGs were precipitated with alcian blue from tissue protein extracts obtained as described above (sGAG assay; Kamiya Biomedical, Thousand Oaks, CA). Point-to-point curve fitting of the standard curve was performed by using the Softmax software (Molecular Devices, Sunnyvale, CA). To ensure accuracy of the low mutant PG values, precipitated PGs from three aliquots of a mutant sample were pooled and measured. All values were normalized to total protein. For disaccharide analyses, liver pieces (≈0.5 g) were frozen in liquid nitrogen, smashed, defatted with acetone, rinsed with ethyl ether, and dried. Lyophilized tissue was weighed and digested with pronase (46). After pronase inactivation and benzonase treatment, the digested PGs were isolated by using DEAE-Sephacel chromatography. Samples were subjected to β-elimination (47). After neutralization with glacial acetic acid, GAGs were precipitated with ethylic alcohol. The final pellet was dried under vacuum and resuspended in H$_2$O. Disaccharide analyses were performed by using heparin lyase digestion, separation by HPLC on a Dionex ProPac PA1 anion exchange column, and UV and fluorescence detection as described (48, 49). See *SI Materials and Methods*.

MRI Imaging. MRI equipment used at the OMRF Small Animal MRI Core Facility was a Bruker (Newark, DE) Biospec 7.0 Tesla/30-cm horizontal-bore imaging spectrometer. Anesthetized mice were placed in an MR probe (35-mm multirung RF volume coil), and livers were localized by MRI. Mouse livers and kidneys were imaged *in vivo* at ages indicated. With the available MRI equipment, cysts as small as 0.12 mm (120 μm) in diameter would be detected. Respiratory gating was used to trigger acquisition of the phase-encoding steps in the imaging sequence for the images. Multiple 1H MR image slices were taken in the transverse plane using a spin-echo multislice (repetition time 1.1 sec, echo time 11.6 msec, 128 × 128 matrix, five steps per acquisition, 3 × 3 cm^2 field of view, 1.3 mm slice thickness).

Blood Chemistry Analyses. Serum chemistries were measured by using an Ortho Diagnostics Systems (Raritan, NJ) Vitros-250 chemistry analyzer machine. For liver function, serum aspartate aminotransferase, alanine aminotransferase, alkaline phosphatase, and lactic dehydrogenase activities were obtained. See *SI Materials and Methods*.

Statistical Analyses. For the incidence of hydronephrosis and incidence of tubule dilation, a two-tailed Fisher's exact test was performed, and other tests of significance unless stated otherwise were done by using one-way ANOVA using JMP software version 5.0.2.1 (SAS Institute, Cary, NC).

Condac *et al.*

www.manaraa.com

1. Boucher C, Sandford R (2004) *Eur J Hum Genet* 12:347–354.
2. Burn TC, Connors TD, Dackowski WR, Petry LR, Van Raay TJ, Millholland JM, Venet M, Miller G, Hakim RM, Landes GM, *et al.* (1995) *Hum Mol Genet* 4:575–582.
3. Harris PC, Ward CJ, Peral B, Hughes J (1995) *J Am Soc Nephrol* 6:1125–1133.
4. Harris PC, Ward CJ, Peral B, Hughes J (1995) *Hum Mol Genet* 4:1745–1749.
5. Hughes J, Ward CJ, Peral B, Aspinwall R, Clark K, San Millan JL, Gamble V, Harris PC (1995) *Nat Genet* 10:151–160.
6. Mochizuki T, Wu G, Hayashi T, Xenophontos SL, Veldhuisen B, Saris JJ, Reynolds DM, Cai Y, Gabow PA, Pierides A, *et al.* (1996) *Science* 272:1339–1342.
7. Torres VE, Harris PC (2006) *Nat Clin Pract Nephrol* 2:40–55.
8. Wilson PD (2004) *N Engl J Med* 350:151–164.
9. Wilson PD (1996) in *Polycystic Kidney Disease*, eds Watson ML, Torres VE (Oxford Univ Press, Oxford), pp 124–163.
10. Carone FA, Bacallao R, Kanwar YS (1996) in *Polycystic Kidney Disease*, eds. Watson ML, Torres VE (Oxford Univ Press, Oxford), pp 111–124.
11. Drenth JP, Martina JA, van de Kerkhof R, Bonifacino JS, Jansen JB (2005) *Trends Mol Med* 11:37–42.
12. Calvet JP (1993) *Kidney Int* 43:101–108.
13. Calvet JP (2003) *Proc Natl Acad Sci USA* 100:5583–5585.
14. Cuppage FE, Huseman RA, Chapman A, Grantham JJ (1980) *Kidney Int* 17:372–381.
15. Igarashi P, Somlo S (2002) *J Am Soc Nephrol* 13:2384–2398.
16. Mangoo-Karim R, Sullivan L, Ye M, Grantham JJ (1996) in *Polycystic Kidney Disease*, eds Watson ML, Torres VE (Oxford Univ Press, Oxford), pp 39–62.
17. Milutinovic J, Agodoa LC, Cutler RE, Striker GE (1980) *Am J Clin Pathol* 73:740–747.
18. Murray SL, Grubman SA, Perrone RD, Rojkind M, Moy E, Lee DW, Jefferson DM (1996) *Connect Tissue Res* 33:249–256.
19. Shannon MB, Patton BL, Harvey SJ, Miner JH (2006) *J Am Soc Nephrol* 17:1913–1922.
20. Zhang Q, Taulman PD, Yoder BK (2004) *Physiology (Bethesda)* 19:225–230.
21. Hacker U, Nybakken K, Perrimon N (2005) *Nat Rev Mol Cell Biol* 6:530–541.
22. Esko JD, Selleck SB (2002) *Annu Rev Biochem* 71:435–471.
23. Proudfoot AE, Handel TM, Johnson Z, Lau EK, LiWang P, Clark-Lewis I, Borlat F, Wells TN, Kosco-Vilbois MH (2003) *Proc Natl Acad Sci USA* 100:1885–1890.
24. Iozzo RV (2005) *Nat Rev Mol Cell Biol* 6:646–656.
25. Cuellar K, Chuong H, Hubbell SM, Hinsdale ME (2007) *J Biol Chem* 282:5195–5200.
26. Ponighaus C, Ambrosius M, Carrera Casanova J, Prante C, Kuhn J, Esko JD, Kleesiek K, Gotting C (2007) *J Biol Chem* 282:5201–5206.
27. Voglmeir J, Voglauer R, Wilson IB (2007) *J Biol Chem* 282:5984–5990.
28. Gotting C, Kuhn J, Zahn R, Brinkmann T, Kleesiek K (2000) *J Mol Biol* 304:517–528.
29. Fausto N, Campbell JS (2003) *Mech Dev* 120:117–130.
30. Gabow PA (1993) *N Engl J Med* 329:332–342.
31. Germino GG, Chapman AB (2001) in *The Metabolic Basis of Inherited Disease*, eds Scriver CR, Valle AD, Sly WS, Childs B, Kinzler KW, Vogelstein B (McGraw–Hill, New York), pp 5467–5489.
32. Wu G, Tian X, Nishimura S, Markowitz GS, D'Agati V, Park JH, Yao L, Li L, Geng L, Zhao H, *et al.* (2002) *Hum Mol Genet* 11:1845–1854.
33. Carone FA, Nakamura S, Punyarit P, Kanwar YS, Nelson WJ (1992) *J Am Soc Nephrol* 3:244–253.
34. Fry JL, Jr, Koch WE, Jennette JC, McFarland E, Fried FA, Mandell J (1985) *J Urol* 134:828–833.
35. Saadi-Kheddouci S, Berrebi D, Romagnolo B, Cluzeaud F, Peuchmaur M, Kahn A, Vandewalle A, Perret C (2001) *Oncogene* 20:5972–5981.
36. Husson H, Manavalan P, Akmaev VR, Russo RJ, Cook B, Richards B, Barberio D, Liu D, Cao X, Landes GM, *et al.* (2004) *Genomics* 84:497–510.
37. Rankin CA, Suzuki K, Itoh Y, Ziemer DM, Grantham JJ, Calvet JP, Nagase H (1996) *Kidney Int* 50:835–844.
38. Guay-Woodford LM (2003) *Am J Physiol Renal Physiol* 285:F1034–F1049.
39. Fujita M, Spray DC, Choi H, Saez JC, Watanabe T, Rosenberg LC, Hertzberg EL, Reid LM (1987) *Hepatology* 7:1S–9S.
40. Monga SP, Micsenyi A, Germinaro M, Apte U, Bell A (2006) *Cell Tissue Res* 323:71–79.
41. Zeisberg M, Kramer K, Sindhi N, Sarkar P, Upton M, Kalluri R (2006) *Mol Cell Biochem* 283:181–189.
42. Handel TM, Johnson Z, Crown SE, Lau EK, Proudfoot AE (2005) *Annu Rev Biochem* 74:385–410.
43. Engelhardt NV, Factor VM, Yasova AK, Poltoranina VS, Baranov VN, Lasareva MN (1990) *Differentiation* 45:29–37.
44. Fisher LW, Stubbs JT, III, Young MF (1995) *Acta Orthopaed Scand* 266:61–65.
45. Dutt S, Kleber M, Matasci M, Sommer L, Zimmermann DR (2006) *J Biol Chem* 281:12123–12131.
46. Ledin J, Staatz W, Li JP, Gotte M, Selleck S, Kjellen L, Spillmann D (2004) *J Biol Chem* 279:42732–42741.
47. Warda M, Toida T, Zhang F, Sun P, Munoz E, Xie J, Linhardt RJ (2006) *Glycoconjugate J* 23:555–563.
48. Toyoda H, Yamamoto H, Ogino N, Toida T, Imanari T(1999) *J Chromatogr* A 830:197–201.
49. Turnbull JE (2001) in *Proteoglycan Protocols*, ed Iozzo RV (Humana, Totowa, NJ), pp 141–147.

MEDICAL SCIENCES

Condac *et al.*